The Rheological Behavior of Firn: Experimental Observations of Dislocation Creep via Grain Boundary Sliding

By: D. R. Furman[1]
Advisor: D. L. Goldsby[1]

[1]Department of Earth and Environmental Science, University of Pennsylvania, Philadelphia, PA 19104
Corresponding author: Daniel R. Furman (dfurman@sas.upenn.edu)

Acknowledgements: This work was conducted with the materials and resources in the Penn Experimental Geophysics Laboratory and funded through Penn CURF. We are grateful to Prof. Richard B. Alley for discussions on the near-surface cryosphere, and for inputs from Andrew J. Cross and doctoral student Travis Hager, which greatly improved the experiments, and the content and clarity of the research.

All data and analyses required to replicate the numbers, figures, and models within are shared open access at the following link: https://github.com/daniel-furman/ice-densification-research.

Key Points

- Constant-stress laboratory experiments were performed on H2O ice powder samples with roughly uniform grain sizes varying from 5 to 550 micrometers (μm) in radius.
- Two rheologically-distinct creep regimes emerged, characterized by their stress dependence n and grain size sensitivity p: dislocation creep (n ~ 3.7, p ~ 0) and disGBS (n ~ 1.6, p ~ 0.9).
- Extrapolation of flow laws for disGBS and other creep mechanisms show that disGBS is the rate-limiting mechanism for natural conditions, such as in glaciers and ice sheets.

Key Words

- Ice sheets, glaciers, firn densification, microstructure, grain size sensitivity, dislocation creep, disGBS, the field boundary hypothesis, constant-stress creep tests

Abstract

Firn densifies through a number of processes at the near-surface of ice sheets and glaciers, with diffusion creep and dislocation creep previously identified as operative mechanisms. Here, we performed a series of compaction experiments on ice powder samples synthesized with differing grain size, characterized by ultra-fine (~ 5 μm), fine (~ 17 μm), medium (~ 187 μm), and coarse (~ 550 μm) radii. Mechanical tests were performed at constant stress (0.3 – 1.4 MPa), at a constant temperature (233 K), and between 80 to 90% relative density. Steady-state creep rates were analyzed via a flow law (Eq. 1) with a power-law relationship between the densification rate ($\dot{\varepsilon}$), applied stress (σ), and grain diameter (d) ($\dot{\varepsilon} \propto \frac{\sigma^n}{d^p}$). The creep rates were found to be dependent on grain size in fine- and ultra-fine- grained samples, with a stress exponent n ~ 1.6 and a grain size exponent p ~ 0.9, and independent of grain size in medium- and coarse-grained samples, with n ~ 3.7 and p ~ 0. We show that these data represent two creep mechanisms, disGBS and dislocation creep respectively, as is observed in the flow behavior of solid ice in terrestrial and planetary ice bodies.

Plain Language Summary

Vast deposits of partially dense ice, or firn, form layers in the near-surface of glaciers and ice sheets on earth and in space. To determine the flow properties for these ice bodies, we produced and then deformed samples of ice powder in the laboratory, a controlled setting wherein we isolated (and varied) particular physical variables. Experiments were conducted in the freezer and took anywhere between two hours to fourteen days in total, depending on the rate of deformation. We found that the ice compaction rates were independent of grain size at coarser grain sizes. However, among finer grain sizes, we discovered a mechanism directly sensitive to grain size, meaning that samples composed of ultra-fine grains flowed more rapidly than samples of fine grains. Grain size sensitivity for firn should be further tested and, upon future consensus review, included in glaciological models.

1. Introduction

Firn is defined as polar snow surviving longer than a single melt season, a transition state between snow and solid ice (Baker, 2019). In general, glaciers and ice sheets increase their mass through an accumulation of snow at the surface, which seasonally stratifies into firn layers at depths of up to ~80 m. The firn column requires anywhere from hundred(s) to several thousands of years to fully densify in terrestrial settings (Ebinuma and Maeno, 1987, Schwander et al., 1997).

Near-surface densification is an important process with implications for understanding the cryosphere's climate records. Trapped gases hundreds of thousands of years into the past are contained within glaciers and ice sheets; however, dating uncertainties arise from the time lag between younger atmospheric gases that permeate the firn down to the bubble close off depth and the older age of the ice at the close off depth (Faria et al., 2010, Adolph & Albert 2014). Glaciologists typically turn to models to date ice records by determining rates of densification, backing out the time it took for pores to become disconnected from one another and from the atmosphere (Wilkinson 1988). Densification models are also critical for determining the overall mass of ice bodies, particularly from measurements of surface elevation from satellites, which are influenced by the density structures of near-surface ice in the conversion of volume to mass (Li et al., 2011, Lenaerts et al., 2019, Keenan et al., 2020).

Ice deforms through steady-state viscous flow, or creep, in low deviatoric stress environments common to the cryosphere (Goldsby 2006). Ice creeps at rates that far exceed its theoretical strength, a phenomenon linked to the presence of lattice defects - dislocations - in the ice. Dislocation creep mechanisms refer to modes of deformation that move dislocations through the material, dominant in ice, metals, alloys, and other materials. Steady-state creep is described by constitutive equations (flow laws), which are relationships between the creep rate ($\dot{\varepsilon}$) and the applied stress (σ) (with $\dot{\varepsilon} \propto \sigma^n$). In expanded form, the flow law includes the environmental conditions and material properties of influence on creep rate (e.g., Eq. 1), such as temperature and grain size (e.g., Goldsby 2006). Ice's material properties include its grain size (Figure 1b), particle-pore geometry, crystallographic preferred orientation, and impurity content (Freitag et al., 2013, Faria et al., 2014), all of which may influence firn's creep rate. The flow law includes quantifiable parameters that encode each material's unique response to the deformation conditions, such as the power law exponents for stress (n) and grain size (p). These parameters are determined directly from laboratory data, with rheological testing as described herein and, for example, by Goldsby and Kohlstedt (2001) and Durham et al. (2001). In contrast, empirical models for firn densification (e.g., Herron, and Langway, 1980) overlook the constitutive physical relationships and are based instead on compaction data from field measurements. This class of models is highly tuned to its training data, and, while they perform well

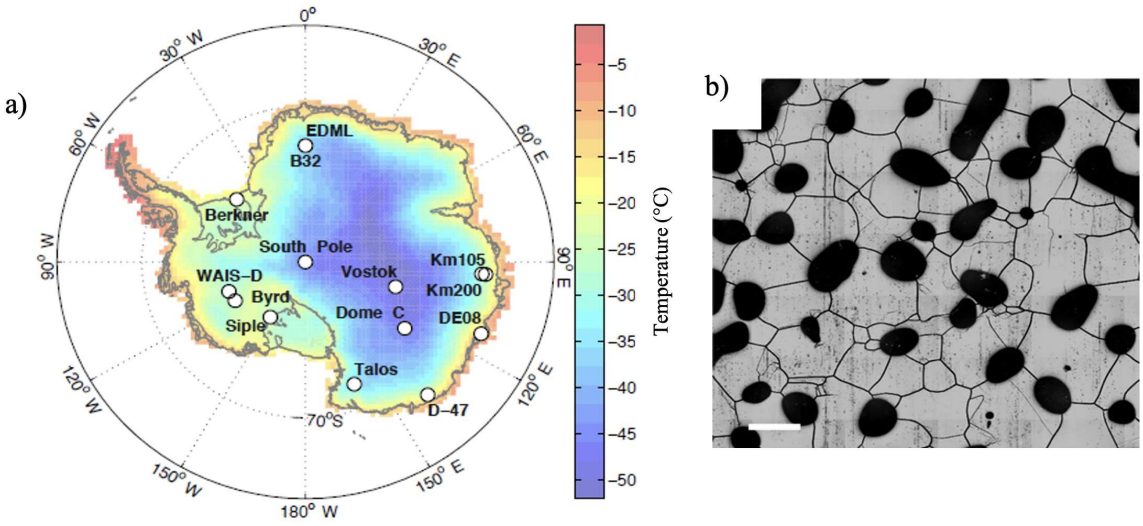

Figure 1. *(a) Map of Antarctica's average annual surface temperature, from Breant et al. (2017). Notice that our 233 K experimental temperature (-40 °C) is a common temperature in the interior regions. Density-stress profiles from Byrd, Dome C, Vostok, Mizuho (NE Antarctica), and GISP-2 (Greenland) are explored herein. (b) Firn from the EDML site at 70 m depth, from Faria et al. (2014) (scale bar = 1 mm). The pore space and grain boundaries are both in black. Dynamic recrystallization processes may have nucleated the smallest grains (r ~ 0.1 mm).*

when extrapolated to similar conditions, empirical models are hindered in extrapolation to novel conditions (Spencer and Alley, 2001, Schultz et al., 2021). This leads to the hypothesis that a physics-based modeling approach is preferred for many glaciological applications (Wilkinson 1988, Keenan et al., 2020), such as dating trapped gas records compacted under conditions absent from the field today, so long as the flow law accurately captures the operative mechanisms at play.

Firn densification occurs in ice with three distinct geometries, with the latter two dominated by steady-state creep. The primary stage consists of frictional grain rearrangement, vapor phase and surface diffusion, as well as melting and refreezing (Maeno and Ebinuma, 1983, Alley, 1987, Schultz et al., 2021). Steady-state creep becomes rate-limiting for both the intermediate and final stage geometries, meaning that creep dominates the overall rate of deformation. For the intermediate stage, the relative density (ρ_r) varies between 80 and 90% of the density of solid ice (Maeno and Ebinuma, 1983). The pore network remains interconnected until pore closure, i.e., at the boundary between the intermediate and final stages. Creep rates for terrestrial ice sheets at the intermediate stage vary from $1e^{-11}$ to $1e^{-12}$ (s^{-1}), as measured by the rate of change in density ($\dot{\rho}/\rho_{ice}$) (Wilkinson and Ashby, 1975). These values were resolved from five density-stress field profiles spanning the terrestrial cryosphere from Antarctica to Greenland (Ebinuma and Maeno, 1987) (Figure 1a). Overall, cumulative strains often reach tens of percent in the firn column, much larger than those characteristic to solid ice creep (Faria et al., 2014, pers. comm., R. Alley, 2020). The firn network develops stress localizations as a result, which in turn activates a number of dynamic microstructural processes (Figure 1b) (Kipfstuhl et al., 2009, Faria et al., 2014).

New experiments exploring firn creep are warranted for many reasons. Contributions from grain-size-sensitive and grain-size-insensitive creep mechanisms are common to natural settings (DeBresser et al., 1998), yet most previous firn flow laws lack this feature (Maeno and Ebinuma, 1983, Wilkinson, 1988, Meussen et al., 1999). For example, disGBS (dislocation-accommodated grain boundary sliding) and dislocation creep both contribute to olivine's densification rate in crustal magma systems (Yao et al., 2019). Previous firn flow laws simply consider one mode of grain-size-insensitive creep (i.e., classical dislocation creep), with the Glen law $n = 3$ stress exponent (Glen 1952, 1955). These models overlook the grain size

sensitivity observed between firn's stratified layers in the field (e.g., Alley, 1982) and the grain size sensitivity observed in solid ice creep (Goldsby and Kohlstedt, 2001, Durham et al., 2001). Overall, this study was predicated on the possibility that we might observe new forms of grain-size-sensitive compaction by testing a range of fine-grained samples.

2. Methods

2.1 Starting Material

Powdered ice of nearly uniform grain size was pressed into a dead-weight-loaded compaction die, to the onset of intermediate stage densification ($\rho_r = 0.8$). Ultra-fine-grained samples of ~5 µm grain radius (Qi et al. 2018) were synthesized by spraying a mist of distilled water through an aerating nozzle into a bath of liquid nitrogen, which was eventually evaporated from the accumulated grains. Fine-, medium-, and coarse-grained samples of ~17, 187, and 550 µm radii were synthesized by crushing distilled-water ice cubes in a kitchen blender. The resulting powder was then sieved to the specified grain size, while occasionally clearing clogged gaps in the mesh with an air gun and by pouring liquid nitrogen over the sieve (Goldsby and Kohlstedt, 2001). The powders were funneled into the die (with a 1-inch diameter) and pressed to an initial porosity near the onset of the intermediate stage, ~80% relative density.

2.2 Compaction Tests

The compaction die (Figure 2a/b) was loaded with weights to a constant applied stress. However, our experiments were not truly constant stress, as the contact area of grains supporting the load increased during densification. Displacement data were recorded with a DC-powered linear variable displacement transducer (LVDT) at a sampling rate of 0.001 Hz. Time-series densification curves were determined from the volume of the sample, which was measured continuously, and the sample mass, which was determined after testing. The data revealed a transient response followed by steady-state creep; for the latter, densification occurred at a constant creep rate (i.e., the sample compacted linearly with time). Densification rates for steady-state creep ($\dot{\rho}/\rho_{ice}$) (s^{-1}) were resolved from the time-series slope, calculated in aggregation to match the densification curve (Appendix Jupyter Notebook, Section 1). Rates corresponded to relatively small changes in density; therefore, the mean relative density was considered representative for the measurement. In addition, interconnected air pockets were assumed to support a negligible load, and pore pressures were ignored due to the channel interconnectivity. Thus, the compressing load was transformed to the applied stress (σ/ρ_r), which ranged from 0.3 to 1.4 MPa, to correct for the area of pore contacts with the piston surface. Some tests were performed under a single applied stress, yielding one rate measurement, while other experiments, particularly those with relatively small rates of deformation, included steps in applied stress.

The die sat in a relatively large freezer held at a fixed temperature of 233 K for each experiment, representative of Antarctic firn temperatures (Figure 1a). The temperature variation for our tests was less than one degree Celsius. Variations in temperature may have exceeded the one-degree limit solely at the beginning and end of an experiment, when the top of the freezer was open; thus, these portions were clipped from the densification curve outputs. For each experiment, the bore was first cleaned with ethanol and then lubricated with molybdenum disulfide spray, minimizing friction between the sample and the die. In addition, the piston was inspected for smoothness and polished with fine sandpaper to remove any burrs. It is also worth noting that any lateral forces resulting from the sample's expansion were minimized by performing experiments at relatively low applied stress.

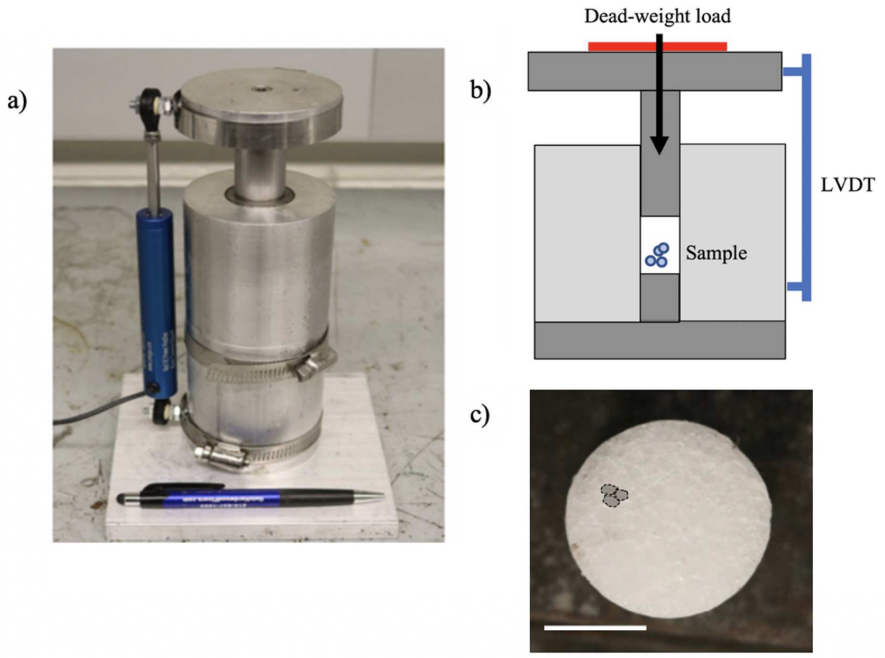

Figure 2. *(a) Photograph of dead-weight compaction die used for creep tests and (b) a corresponding diagram. (c) Photograph of a coarse-grained sample, post-compaction (white scale bar = 0.5 inches). Close inspection of the surface reveals three individual grains (shaded and outlined in black).*

3. Results

We measured sixteen total creep rates across ultra-fine, fine, medium, and coarse series (grain radius ~ 5, 17, 187, 550 μm), color-coded onto Figure 3's data. The steady-state creep results reveal two distinct mechanisms, with the slope of the linear regression corresponding to the stress exponent n ($\dot{\varepsilon} \propto \sigma^n$) across log-log $\dot{\varepsilon}$-σ space. The n exponents for the fine and ultra-fine series of samples ($n = 1.57 \pm 0.22$, $n = 1.68 \pm 0.45$) suggest the operation of a common mechanism, with an average stress exponent of $n = 1.63 \pm 0.34$. The rate differences between the ultra-fine- and fine-grained series indicate the mechanism's grain size sensitivity. A distinct n exponent emerged for the medium-grained samples ($n = 3.74 \pm 1.02$), with the overlapping data indicative of this mechanism's grain size insensitivity. Uncertainties for the n exponents were determined from the 95% confidence intervals of the linear regression. The mean relative density for the rate measurements were kept nearly consistent within each series (ρ_r = $0.831 \pm 5.6e^{-3}$, $0.818 \pm 7.1e^{-3}$, $0.815 \pm 3.3e^{-3}$), essential as the density is a variable that influences the creep rate (Eq. 1). These means and 95% confidence intervals were estimated from bootstrap resampling of the relative density measurements. Experiments were conducted at a relatively low temperature (233 K) to avoid pre-melt along grain boundaries (Goldsby, 2006) and grain growth.

The creep rates were analyzed with the intermediate stage flow law for viscous creep (Wilkinson and Ashby, 1975, Maeno and Ebinuma, 1983), modified to include the grain-size dependence observed in our compaction experiments (Eq. 1). The densification flow law includes the creep rate $\dot{\varepsilon}$, material constant A, applied stress σ, grain size diameter d, temperature T, activation energy Q, gas constant R, n and p exponents, and relative density ρ_r. The power law relationship between creep rate and grain size ($\dot{\varepsilon} \propto d^{-p}$) was added to the original model derived by Wilkinson and Ashby (1975), with the material constant A cancelling the newly introduced units. When p is non-zero, the grain size power law alters the numerical behavior of the model, for example, subtly weakening the dependence of creep rate on density. Further research is warranted to encapsulate the grain size dependence in our

$$\dot{\varepsilon} = \frac{2A(1-\rho_r)}{\left\{1-(1-\rho_r)^{\frac{1}{n}}\right\}^n}\left(\frac{2\sigma}{n}\right)^n exp\left(-\frac{Q}{RT}\right)d^{-p} \quad \text{[Eq. 1]}$$

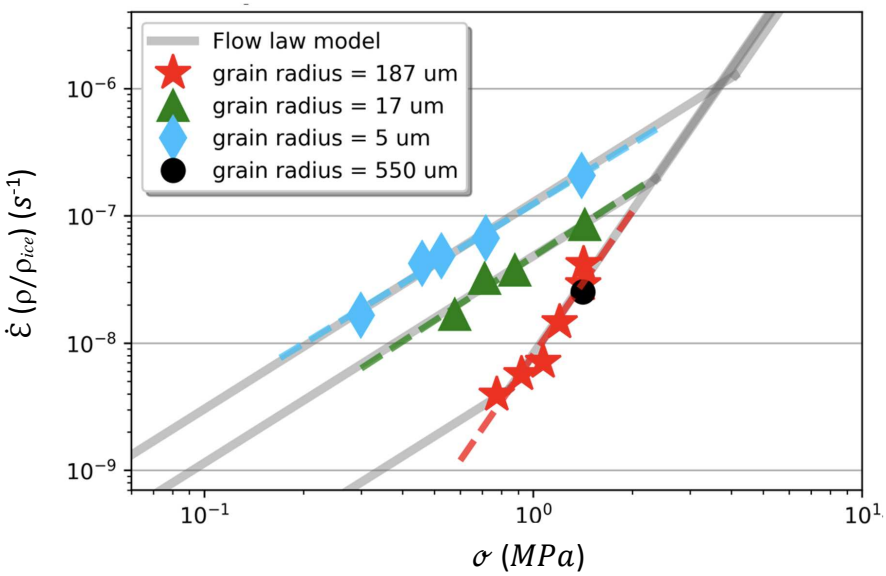

RESEARCH

Figure 3. *Creep rate versus applied stress, in log-log transformed space. The data constrain our flow law (grey lines) by resolving the rate-limiting mechanism. The stress exponents (n ~ 1.6, n ~ 1.7, n ~ 3.7) are taken from the slope of the linear regression (dashed lines).*

compaction data without altering the numerical behavior of the original flow law.

4. Discussion

A disGBS regime and dislocation creep regime were observed for fine and medium-grained samples., respectively, a result consistent with flow laws for solid ice creep (Goldsby, 2006). This leads us to the hypothesis that both mechanisms contribute to the overall creep in natural settings (Behn et al., 2021), particularly for firn columns with grain size distributions significantly deviated around their mean.

4.1 An Updated Framework for Firn Creep

The data in the medium- to coarse-grained regime can be fit with a stress exponent of $n = 3.74 \pm 1.02$, and a pre-exponential term $A \sim 1.48e^{5}$, with the activation energy set to the solid-ice equivalent (Q = 60 kJ/m) (Goldsby, 2006). Dislocation creep exhibits a negligible grain size dependence ($p \sim 0$), evidenced by the overlap between medium- and coarse-grained data (Figure 3). Additionally, the stress exponent for the medium-grained mechanism may more closely match dislocation creep ($n = 4$) in solid ice (Goldsby and Kohlstedt, 2001, Durham et al., 2001), with bootstrap resampling among the medium-grained series yielding a $n \sim 4$ estimate of the mean. In contrast, the fine-grained mechanism fits a stress exponent $n = 1.63 \pm 0.34$, a grain size exponent $p \sim 0.9$, and a material constant $A \sim 0.44$.

These values match well with those for disGBS in fully dense ice, where $n = 1.8$ and $p = 1.4$ (Goldsby and Kohlstedt, 2001, Durham et al., 2001). The disGBS mechanism occurs through grain boundary sliding accommodated by the passage of dislocations along basal slip systems (Goldsby, 2006). The close match between these values of the stress exponent in our tests and for creep of solid ice deforming by disGBS strongly suggests that the mechanism is the same in both cases, as the stress exponent is considered a fundamental property of the steady-state creep mechanism (Wilkinson and Ashby, 1975). Solid ice's $p = 1.4$ grain size exponent, in contrast, is significantly different from our results for firn densification, over 50% higher than the value of $p \sim 0.9$ in our experiments. This is perhaps due to the differences in firn's microstructure compared with solid ice; particularly, in firn, grains have much more freedom to move than in solid ice. The firn grains' proclivity to move perhaps makes it more difficult to develop pinned triple grain junctions compared to solid ice, a key factor for disGBS creep (Goldsby and Kohlstedt, 2001). We assume the activation energy is equivalent to disGBS in solid ice (Q = 49 kJ/mol) (Goldsby, 2006), as was assumed for dislocation creep in the previous firn flow laws (Ebinuma and Maeno, 1983, Wilkinson 1988).

The experimental grain size sensitivity was clearly distinct from diffusion creep mechanisms, which exhibit differing flow law parameters ($n = 1$,

p = 2/3) (Nabarro, 1948, Herring, 1950, Coble, 1963, Coble, 1970). While diffusion creep is dominated by other mechanisms in most natural settings (Wilkinson 1988), it is nevertheless still operative during deformation (Duval et al., 1983, Burr et al., 2019). However, we chose to ignore diffusion creep here, as its flow law contains uncertainty due to a lack of confirmation in laboratory experiments. In addition, other grain-size-sensitive mechanisms may contribute to firn creep, with their identification subject to future testing across expanded laboratory conditions.

4.2 Extrapolation to Natural Settings

We first extrapolated the flow law to the full range of stresses and grain sizes in terrestrial ice sheets and glaciers (Figure 4a). The disGBS mechanism is rate-limiting with decreasing stress and at finer grain size, and, conversely, dislocation creep is rate-limiting with increasing stress and at coarser grain size. The flow law predictions suffered from at least an order of magnitude overprediction error, suggesting that its application to glaciology is at present premature. This overprediction error is easily observed in Figure 4a's creep rate contours (dashed grey lines); in particular, the range of densification rates for terrestrial ice sheets ($1e^{-11}$ to $1e^{-12}$) correspond to creep rate contours that pass outside of the stress and grain size range for ice sheets (blue box). Secondly, flow was extrapolated directly to the temperature, stress, and density data resolved from Ebinuma and Maeno (1987). The disGBS mechanism rate-limits by approximately half an order of magnitude in the coarse-grained limit (Appendix Jupyter Notebook, Section 6). However, dislocation creep rates were a closer match to the natural densification rates, a contradictory result warranting future inquiry. The model's compatibility with natural firn microstructures is a key advantage of our flow law relative to previous results. Firn's inhomogeneous strain state is well known for developing localized stress concentrations and dynamic recrystallization processes (e.g., grain subdivision, migration recrystallization, and rotation recrystallization) (Faria et al., 2014). It is also important to note that disGBS and dislocation creep are both capable of developing the dislocation structures observed in firn columns. For example, these structures were observed within fine-grained solid ice deformed via disGBS in the laboratory (Goldsby and Kohlstedt, 1997a & 1997b). The disGBS mechanism may also accommodate an impurity dependence for firn creep (Freitag et al., 2013, Breant et al., 2017), akin to the minor impurity dependence observed on ice creep among the Antarctic Meserve Glacier's basal layers (Cuffey et al., 2000a).

The flow law is also applicable to icy planetary bodies in the solar system. In these settings, cold temperatures limit grain growth, as well as the overall creep rate. For example, the icy moons of Jupiter exhibit near-surface temperatures of ~100 K, and rates of densification are further hindered by hydrate sulfate salts (Durham et al., 2001, Durham et al., 2010). Planetary ice sheets also contain near-surface firn densification, such as among the dry ice-rich layered polar deposits at the Martian poles (Arthern et al., 2000, Cassanelli et al., 2015). The viscosity, shape, and age of the Martian caps all indicate the presence of H_2O ice layers alongside layers of CO_2 ice. Our experiments suggest that disGBS is the dominant mechanism for H_2O firn creep on Mars (Figure 4b), at the average surface temperature of the polar ice caps, ~165 K (Nye, 2000). Clathrate hydrates, which are also present here, likely have lower creep rates (Durham et al., 2010) than those for H_2O firn.

Experimental errors may have included unwanted contributions from transient creep to steady-state creep (e.g., Durham et al., 2001) and the unconstrained confidence intervals on our sample's grain size distributions. The latter was due to the delay of Scanning Electron Microscope imaging, which also resulted in the unconstrained confidence intervals for disGBS A and p flow law parameters. If we assume the ultra-fine-grained series experienced grain growth to an average radius of 8 μm, the flow law's overprediction errors are drastically reduced and more closely match natural densification rates. Under this scenario, dislocation creep becomes rate-limiting across roughly half of the natural conditions, a picture more consistent with the field boundary hypothesis (DeBresser et al., 1998). The field boundary hypothesis posits that grain-size-sensitive and grain-size-insensitive creep mechanisms contribute in roughly equal proportion to the total rate in natural settings. As such, our multi-mechanism flow law should, in practice, predict the creep rate as a function of the grain size distribution at a given

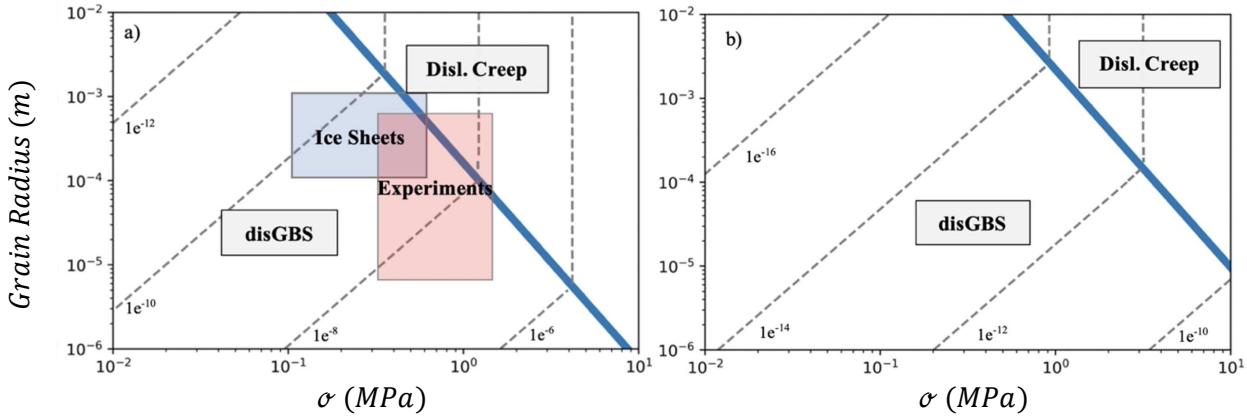

Figure 4. *(a) Mechanism map for intermediate stage densification (ρ_r = 0.85) in the terrestrial cryosphere (233 K), plotted across grain size and stress, after Goldsby (2006). The dashed lines are creep rate contours ($\dot{\rho}/\rho_{ice}$) (s^{-1}) and the blue line is the proposed mechanism regime change (b) Mechanism map for intermediate stage densification (ρ_r = 0.85) in the Martian polar layered deposits (for H_20 firn) (165 K), with its rate contours and regime change also plotted. Here, firn is expected to creep under lower stresses and grain sizes relative to (a) (Durham et al., 2010), rendering disGBS as predominately rate-limiting.*

site, assuming detailed data on grain size distributions are known. Modeling errors may have included an overestimation of the applied stress, as the macroscopic values derived from the ice sheet's density-stress profiles were likely born only by a subset of the firn grains directly neighboring pore channels (Wilkinson, 1988, Faria et al., 2014). In addition, the stress may decrease in response to variations in pore pressure, which were ignored herein due to the channel interconnectivity during the intermediate stage (Maeno and Ebinuma, 1983, Wilkinson, 1988). Lastly, disGBS may invoke more intricate physical considerations of firn's microstructural state, such as limitations for disGBS for finer grains directly neighboring coarser grains.

5. Summary

We developed a physics-based flow law for firn creep with parameters directly constrained from our laboratory data on ice powder densification. We identified two distinct mechanisms in the laboratory, with classical grain-size-insensitive dislocation creep observed for the medium- and coarse-grained samples, and grain-size-sensitive disGBS observed from fine and ultra-fine-grained samples. Upon extrapolation to natural settings, the flaw law predicts dislocation creep and disGBS as rate-limiting mechanisms for higher and lower stress conditions, respectively. Our two-mechanism flow law is similar in form to that for solid ice rheology, unifying the steady-state creep framework for ice sheets and glaciers from near-surface firn densification to ice flow at depth.

References

Adolph, A. C., Albert, M. R.: Gas diffusivity and permeability through the firn column at Summit, Greenland: measurements and Comparison to microstructural properties, *The Cryosphere*, 8(1), 319-328, 2014.

Alley, R. B.: Polar Firn Densification and Grain Growth. *Annals of Glaciology*, 3, 7-11, 1982.

Alley, R. B.: Firn densification by grain boundary sliding: a first model, *J. de Physique*, 48(3), 1987.

Alley, R. B.: Transformations in Polar Firn, PhD Thesis U. of Wisconsin-Madison Dpt. of Geology, p. 88, 1987.

Arthern, R. J., Winebrenner, D. P., & Waddington, E. D.: Densification of Water Ice Deposits on the Residual North Polar Cap of Mars, *Icarus*, 144(2), 367-381, 2000.

Baker I.: Microstructural characterization of snow, firn and ice*, Phil. Trans. Royal Society A*, 377, 2019.

Behn, M. D., Goldsby, D. L., and Hirth, G.: The role of grain-size evolution on the rheology of ice: Implications for reconciling laboratory creep data and the Glen flow law, *The Cryosphere Discuss.* [preprint], in review, 2020.

Breant, C., Martinerie, P., Orsi, A., Arnaud, L. & Landais, A.: Modelling firn thickness evolution during the last deglaciation: constraints on sensitivity to temperature and impurities, *Climate of the Past*, 13(7), 833–853, 2017.

Burr, A., P. Lhuissiera, C. L. Martina & A. Philip.: In situ X-ray tomography densification of firn: The role of mechanics and diffusion processes, *Acta Materialia*, 167, 210-220, 2019.

Cassanelli, J. P, and Head, J. W.: Firn densification in a Late Noachian "icy highlands" Mars: Implications for ice sheet evolution and thermal response, *Icarus*

253, 243-255, 2015
Coble, R.L.: A model for boundary diffusion controlled creep in polycrystalline materials, *J. of Appl. Physics*, 34(6), 1679-1682, 1963.
Coble, R.L.: Diffusion Models for Hot Pressing with Surface Energy and Pressure Effects as Driving Forces, *J. of Appl. Physics*, 41(12), 1970.
Cuffey, K., Conway, H., Gades, Anthony, Hallet, B., Raymond, C., & Whitlow, S.: Deformation properties of subfreezing glacier ice: Role of crystal size, chemical impurities, and rock particles inferred from in situ measurements, *J. of Geophys. R. Solid Earth* , 105(B12), 27895-27915, 2000.
De Bresser, J.H.P., C.J. Peach, J.P.J. Reijs & C.J. Spiers: On dynamic recrystallization during solid state flow: Effects of stress and temperature, *Geophys. Res. Letters*, 25(18), 3457– 3460, 1998.
Durham, W. B., L. A. Stern, & S. H. Kirb.: Rheology of ice I at low stress and elevated confining pressure, *J. of Geophys. Research,* 106(11), 11031-11042, 2001.
Durham, W.B., Ballesteros, O. & Goldsby, D.L.: Rheological and Thermal Properties of Icy Materials, *Space Sci review*, 153(1), 273-298, 2010.
Duval, P., Ashby, M.F., & Anderman, I.: Rate-controlling processes in the creep of polycrystalline ice, *J. Phys. Chem,* 87(21), 4066–4074, 1983.
Ebinuma, T. & Maeno, N.: Experimental Studies on densification and pressure sintering of ice, *Annals of Glaciology*, 6, 83-86, 1985.
Ebinuma, T. & Maeno, N.: Particle Rearrangement and Dislocation Creep in a Snow-Densification Process, *Journal de Physique Colloques*, 48(C1), 263-269, 1987.
Faria, H. F., Freitag, J., & Kipfstuhl, S.: Polar ice structure and the integrity of ice-core paleoclimate records, *Q. Sci. Reviews*, 29(1-2), 338-351, 2010.
Faria, S. H., Weikusat, I., & Azuma, N.: The microstructure of polar ice, Part II: State of the art, *J. of Structural Geology*, 61, 21-49, 2014.
Freitag, Kipfstuhl, Laepple, & Wilhelms: Impurity controlled densification: a new model for stratified polar firn, *J of Glacio.*, 59(218), 1163-1169, 2013.
Frost, H. J., & Ashby, M. F.: Deformation-Mechanism Maps: The Plasticity and Creep of Metals and Ceramics. Oxford: Pergamon Press. 1982.
Glen, J.W.: Experiments on the deformation of ice, *J. of Glacio.*, 2(12), 111- 114, 1952.
Glen, J.W.: The creep of polycrystalline ice, *Proc. R. Soc. London*, 228(1175), 519-538, 1955.
Goldsby, D.L., & D.L. Kohlstedt: Grain boundary sliding in fine-grained Ice I, *Scr. Mater*, 37(9), 1399–1406, 1997a.
Goldsby, D.L., & D.L. Kohlstedt: Flow of ice I by dislocation, grain boundary sliding, and diffusion processes, in Proceedings of the 28th Annual Lunar and Planetary Science Conference (Lunar and Planetary Ins. Houston), 429–430, 1997b.
Goldsby, D.L. & D.L. Kohlstedt: Superplastic deformation of ice: Experimental observations, *J. Geophys. Research*, 106(11), 17-30, 2001.
Goldsby, D.L.: Superplastic flow of ice relevant to glacier and ice-sheet mechanics. Glacier Science and Environmental Change. Blackwell Publishing, 2006.
Herring, C.: Diffusional viscosity of a polycrystalline solid, *J. Appl. Physics*, 21, 437-444, 1950.
Herron, M. M. & C. C. Langway, Jr.: Firn densification: an empirical model, *J. of Glacio.,* 25(93), 373-385, 1980.
Keenan, E., Wever, N., Dattler, M., Lenaerts, J. T. M., Medley, B., Kuipers Munneke, P., and Reijmer, C.: Physics- based SNOWPACK model improves representation of near- surface Antarctic snow and firn density, *The Cryosphere*, 15, 1065–1085, 2021.
Kipfstuhl, S., S. H. Faria, N. Azuma, J. Freitag, I. Hamann, P. Kaufmann, H. Miller, K. Weiler, & F. Wilhelms: Evidence of dynamic recrystallization in polar firn, *J. Geophys. Research*, 114, B05204, 2009.
Maeno, N. & Ebinuma, T.: Pressure sintering of ice and its implication to the densification of snow at Polar glaciers and ice sheets, *J. Phys. Chem.*, 87(41), 3-10, 1983.
Meussen, B. Mahrenholtz, & O. Oerter, H.: Creep of Polar Firn, *Cold Regions Science and Technology*, 29, 177-200, 1999.
Nabarro, F.R.N.: Deformation of crystals by the motion of single ions, in Report of a Conference on Strengths of Solids (Bristol), 75- 90, Phys. Soc., London, 1948.
Nye, J. F.: A flow law model for the polar caps of Mars, *J. of Glacio.*, 46(154), 438-444, 2000.
Qi, C., Stern, L. A., Pathare, A., Durham, W. B., & Goldsby, D. L.: Inhibition of Grain Boundary Sliding in Fine-Grained Ice by Intergranular Particles: Implications for Planetary Ice Masses, *Geophys. R. Letters*, 45(23), 12757–12765, 2018.
Schultz, T., Müller, R., Gross, D., and Humbert, A.: On the Contribution of Grain Boundary Sliding to Firn Densification – an Assessment using an Optimisation Approach, *The Cryosphere Discuss*, [preprint], in review, 2021.
Spencer, M. K. & Alley, R. B.: Preliminary Firn Densification Model with 38-site Dataset, *J. of Glacio.*, 47(159), 671-676, 2001.
Wilkinson, D. S. & M. F. Ashby.: Pressure sintering by power law creep, *Acta Metallurgica*, 23(11), 1277-1286, 1975.
Wilkinson, D.S.: A pressure-sintering model for the densification of polar firn and glacier ice, *J. of Glacio.*, 34(116), 1988.
Yao, Z., Qin, K., Wang, Q., & Xue, S.: Weak Btype olivine fabric induced by fast compaction of crystal mush in a crustal magma reservoir, *J. of Geophys. R.: Solid Earth,* 124(4), 3530–3556, 2019.